Chapter 2

Theoretical framework

This chapter presents the pre-requisite theoretical formalisms that were utilized for the current investigation. Various elastic and inelastic cross-sections are calculated for the electron collision with target systems for the energy range 0.1-5000 eV. For low energy calculations (i.e., 0.1-20 eV) R-matrix approach and for intermediate to high energy calculations (i.e., ionisation threshold to 5000 eV) spherical complex optical potential (SCOP) formalism is employed. Complex scattering potential-ionisation contribution (CSP-ic) technique is used to extract out the ionisation cross-sections from the total inelastic cross-sections. Various correlations between the cross-sections and target properties have also been analysed and discussed, leading to the prediction of polarizability and dielectric constant of the targets. The computation methodology in case of condensed or solid phase target systems is also described here.

2.1 Introduction

When human mind encounters the word "scattering," they immediately conjure up an image of two individuals colliding with each other. This vision is a product of the way we look at the world as a whole. On the other hand, nature is incredibly mysterious, and at every scale, there is always something exciting and unexpected to be discovered there. The large-scale (macroscopic) world embodies many particles of micro level, and the concepts/theories that apply in the large-scale universe could not apply in the meticulous micro-scale world. Since many observations overruled the laws of classical physics, quantum mechanics was piecemeal developed to study the microscopic region of our world. Within the realm of quantum mechanics, the term "scattering" refers, in its most fundamental sense, to a change in the trajectory of the projectile that is brought about by the existence of the target particle. When this collision transpires, there are an enormous number of various processes that takes

place. The probability of occurring all of these scattering processes can be quantified through the scattering cross-sections.

2.1.1 Physical interpretation of cross-sections

Consider the standard scattering experiment depicted in figure 2.1, where a uniform and collimated beam of monoenergetic electrons, e^- is aimed at a scatterer (target) X. Additionally, it is presumed that the target behaves as a sole system in order to assure a solitary collision situation. In addition, the amount of time taken by electrons to travel through the interaction area is going to be significantly less than the amount of time it took before the incident beam was activated. This leads to a state of stable operation.

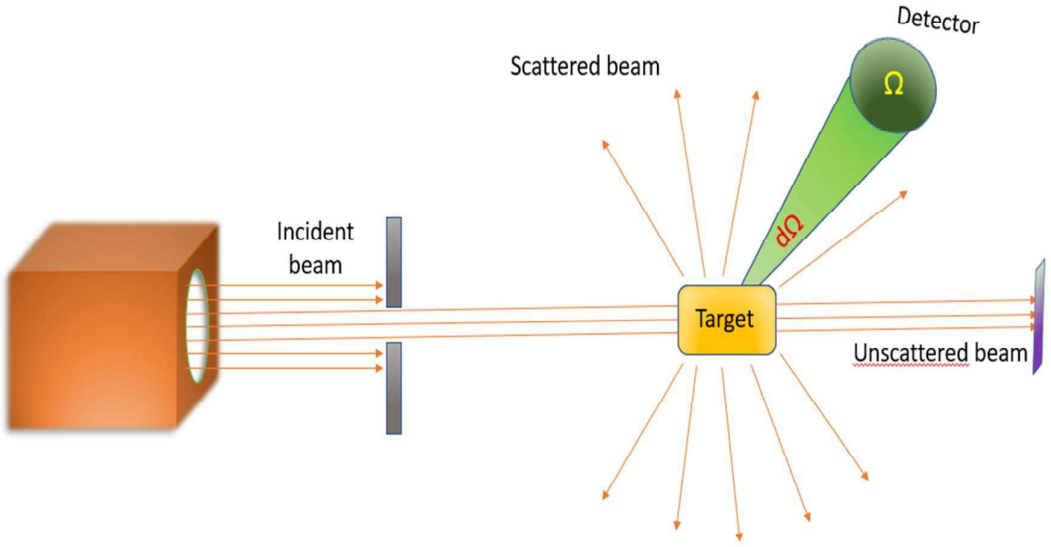

Figure 2.1 Schematic diagram for scattering of projectile particles from target system

Owing to the interaction between the incident beam and the atomic or molecular target, a certain number of scatterers are able to block the path of the incoming beam of electrons. This interruption can just be the result of an interaction among the two charged entities and not an actual physical blockage. This number shall hereafter be referred to as N_X. Now, a particular effective region of the scatterers will block the path that the incident electron is travelling in. Let A represent the effective region that is obstructed by N_X scatterers. Let N_e be the number of incident electrons that reach the target X per unit of time. Only a certain fraction of these N_e will engage in interaction with the X system. The notation "N_{in}" is used to refer to this quantity per unit of time. It should be evident that this represents a portion of N_e.

This fraction is dependent on the probability of the occurrence of the interaction between the electrons and scatterers. Let us refer this as *P*, which stands for the probability that an electron in the incident flux will interact with the scatterer and, as a result, be removed from the incoming flow via scattering.

$$N_{in} = P \times N_e \tag{2.1}$$

This N_{in} will be directly influenced by the incoming flux $\left(\emptyset_e = {}^{N_e}/_{A}\right)$ and N_X,

$$N_{in} \propto \emptyset_e \cdot N_X \tag{2.2}$$

$$N_{in} = Q \cdot \emptyset_e \cdot N_X \tag{2.3}$$

$$Q = \frac{P \cdot N_e}{\emptyset_e \cdot N_X} \tag{2.4}$$

This Q is referred to as the scattering cross-section, and its physical dimension is [L^2]. It provides a measurement of the propensity of electrons and target *X* to interact and thus, is proportional to the probability of an interaction. *Cross section refers to the effective target area that intercepts and scatters the projectile's incident beam* [1].

2.1.2 Optical Theorem

The Schrödinger equation needs to be solved in order to find a solution to any scattering issue. The equation is given as follows,

$$-\frac{\hbar^2}{2m}\nabla^2\Psi(r) + V(r)\,\Psi(r) = E\,\Psi(r) \tag{2.5}$$

Ψ here describes the system's state. The complete solution to this equation is comprised of two waves: a scattered wave and an incident wave. It is considered that the wave associated with the scattered particles was spherically symmetric and recedes with the distance. The incoming wave was presumed to be a plane wave. Therefore, the scattered wave should take the form of $\left({}^{1}/_{r}\right)$, with the area $\left({}^{1}/_{r}\right)^2$ decreasing to 0 (zero) as $r \to \infty$ in the asymptotic region. Given that the detector is located at such a considerable distance from the scattering system that it is considered to be infinite, thus this particular distance is of relevance. As a result, to find a solution of any scattering problem, we must explore the solution in this region. In addition, the amplitude of the scattering will be dependent on a specific angle (θ, φ or Ω), which indicates the direction in which the scattering takes place. The equation for the total wave (comprised of both the scattered and incident wave) is written as,

$$\lim_{r\to\infty} \Psi(r) = C\left[e^{(ik_0 r)} + f(\theta,\varphi)\frac{e^{(ikr)}}{r}\right] \tag{2.6}$$

where, C is the normalisation constant, the wave vectors for incident and scattered wave are k_0 and k, respectively. The scattering amplitude is denoted by $f(\theta,\varphi)$. Here, θ is the angle between k_0 and k.

Consider the probability current density as,

$$\mathrm{J}(r) = Re\left[\frac{\hbar}{im}\Psi^*(r)\cdot\nabla\Psi(r)\right] \tag{2.7}$$

Taking into account the radial component and neglecting the $\left(1/r^2\right)$ term compared to the $\left(1/r\right)$, the solution provides three terms that correspond to the incoming flux, the interference flux and the outgoing flux. A plane wave is taken into account while describing the incident term. It behaves like a pure incoming wave, as if there is no scattering at all, whatever enters the system leaves the system. Hence, the incident term vanishes. Thus, for the steady state expression,

$$\int \mathrm{J}_{out}(r)\cdot da + \int \mathrm{J}_{inter}(r)\cdot da = 0 \tag{2.8}$$

The solution provides as follows, by considering the outgoing term [1],

$$\int \mathrm{J}_{out}(r)\cdot da = \frac{\hbar k}{m}|C(k)|^2 \int |f(\Omega)|^2\cdot d\Omega \tag{2.9}$$

Now, the single differential cross-section, $\frac{dQ}{d\Omega}$ is defined by the term $|f(\Omega)|^2$. Thus, the above equation is rewritten as

$$\int \mathrm{J}_{out}(r)\cdot da = \frac{\hbar k}{m}|C(k)|^2 Q_T \tag{2.10}$$

At $\theta = 0^o$, where forward scattering occurs, we discover that the interference term becomes significant. This term approaches zero in the asymptotic area, which encompasses all other angles. However, for extremely small angles, the term can be written as

$$\int \mathrm{J}_{inter}(r)\cdot da = \frac{\hbar k}{m}|C(k)|^2 \times 2\pi\, Re\left[f(0)\left\{\frac{i}{k}\right\} + f^*(0)\left\{\frac{-i}{k}\right\}\right] \tag{2.11}$$

$$\int \mathrm{J}_{inter}(r)\cdot da = \frac{\hbar k}{m}|C(k)|^2 \times \frac{-4\pi}{k}\, Im[f(0)] \tag{2.12}$$

From equations 2.8, 2.10 and 2.12,

$$Q_T = \frac{4\pi}{k}\, Im[f(0)] \tag{2.13}$$

The $f(0)$, scattering amplitude at forward angle, and Q_T are related through the equation 2.13, *Bohr-Peierls-Placzek relation*, also clled as the *optical theorem* [1]. The shadow that is cast by the scatterer (target) in the forward direction recedes the intensity of the incident wave, which results in the scattered particles being removed in a manner that is proportional to the Q_T. The theorem's physical foundation is the principle of flux probability conservation. Interference between incident and scattered waves at zero forward angle is responsible for this relationship, as was previously discussed.

2.2 Spherical Complex Optical Potential approach (SCOP)

Any scattering event can be described and solved through the Schrödinger equation (equation 2.5). The potential $V(r)$ that can be incorporated into Schrödinger equation 2.5 will be developed here. This SCOP method is a way for computing the interaction potential, utilised to obtain the scattering cross sections. Before it was applied to collision physics, in the field of nuclear physics, this idea of a complex potential was initially established [2]. The generation of this potential for electron scattering systems will be covered in the following subsections.

2.2.1 Interaction potentials

Elastic and inelastic channels can be used to broadly categorise the events that may occur as a result of the impact of projectile electrons onto the target. Quantification of elastic events can be done using the polarisation, exchange, and static effects and that for inelastic events can be done using absorption effects. A complex potential characterises the dynamics of the collision between the electrons and target; the real component of this potential represents the elastic events, while the imaginary part accounts for the inelastic ones. This is similar to how the complex refractive index works in optics, where the real part of it relates to the portion of the wave that passes through the medium, while the imaginary part represents the portion of the wave that is absorbed by the medium. Therefore, the complex potential will be,

$$V_c(r, E_i) = V_p(r, E_i) + V_{ex}(r, E_i) + V_s(r) + iV_{ab}(r, E_i) \tag{2.14}$$

where, V_p, V_{ex}, V_s and V_{ab} represent the polarisation, exchange, static and absorption potential, respectively. E_i is the incident energy of the projectile electrons.

Charge density and static potential

Poisson's equation, a fundamental tool, allows us to express the correlation between the static potential, V_s and the desired target charged cloud density $\rho(r')$ [3,4] as,

$$V_s(r) = \frac{-Z}{r} + 4\pi \left[\frac{1}{r}\int_0^r \rho(r')\, r'^2 dr' + \frac{1}{r'}\int_0^\infty \rho(r')\, r' dr'\right] \tag{2.15}$$

For a variety of atoms, Cox and Bonham [5] have successfully fitted the radial charged density function by making use of the potential field parameters λ_i and γ_i. The V_s and $\rho(r)$ are given by an analytical form as,

$$V_s(r) = \frac{-Z}{r}\sum_i \gamma_i e^{-\lambda_i r} \tag{2.16}$$

$$\rho(r) = \frac{Z}{4\pi r}\sum_i \lambda_i^2\, \gamma_i\, e^{-\lambda_i r} \tag{2.17}$$

Polarisation potential

Polarisation potential, abbreviated as V_p, is developed when the charge cloud of the target system is momentarily redistributed as a result of the electric field induced by an incoming electron. This results in the production of multipole moments. The possibility for correlation polarisation can be described by a number of various models. This calculation makes use of the parameter-free model that Padial and Norcross [6] suggested,

$$V_p(r) = \begin{cases} \vartheta_{co}(r), & r \le r_c \\ \frac{-\alpha_d}{2r^4}, & r > r_c \end{cases} \tag{2.18}$$

Here, r_c is the first crossing point between the long-range dipole component, $\frac{-\alpha_d}{2r^4}$ and the short-range polarisation component $\vartheta_{co}(r)$.

It has been shown by Perdew and Zunger [7] that,

$$\vartheta_{co}(r) = \begin{cases} 0.033\, ln\, r_S - 0.584 + 0.00133\, ln\, r_S - 0.0084 r_S, & r_S < 1 \\ \frac{-\gamma\left(1+\frac{7}{6}\beta_1\sqrt{r_S}+\frac{4}{3}\beta_2 r_S\right)}{\left(1+\beta_1\sqrt{r_S}+\beta_2 r_S\right)^2}, & r_S \ge 1 \end{cases} \tag{2.19}$$

Here, r_S is the density parameter $\left(= \left(\frac{3}{4\pi\rho(r)}\right)^{1/3}\right)$. The constants $-\gamma, \beta_1$ and β_2 have the values 0.1423 a.u., 1.0523 a.u. and 0.3334 a.u., respectively.

In the vicinity of target, polarisation potential should approach the ϑ_{co}, and it should have the right asymptotic form for larger distance r. In the study of Zhang *et.al.* [8] presented new polarisation potential, which can be stated in mathematical form as,

$$V_{pco}(r) = \frac{-\alpha_d}{2\left(r^2+r_{CO}^2\right)^2} \tag{2.20}$$

Where, the cur-off parameter, r_{CO} can be found by plugging the equation $V_{pco}(r) = {}^{\alpha_d}/_{2r_{CO}^4} = \vartheta_{co}(0)$. This brings V_{pco} close to the asymptotic form for larger distance and makes $V_{pco} = \vartheta_{CO}$ near the target area.

Exchange potential

When there is an electron as a projectile, there is a chance that it will swap places with one of the electrons in target atomic or molecular system that it is aiming at. The potential that results from the fact that electrons cannot be distinguished from one another is handled by employing the exchange potential, V_{ex}. Exchange primarily has the effect of keeping the approaching projectile electron off from the target electron with same spin. By doing so, the whole wavefunction maintains its anti-symmetry regarding the changing of the projectile electron's coordinates with that of the target. Considering the electron to be a Fermi gas that adheres to Pauli's exclusion principle, Hara [9] developed a "free electron gas exchange model", also called as "Hara Free Electron Gas Exchange model", for the purpose of calculating V_{ex}. The amount of energy that is exchanged, is determined by adding together all of the momentum states that go up to the Fermi energy, ε_F. The ultimate realisation of the potential is expressed here as,

$$V_{ex}(r, E_i) = 2\frac{k_F}{\pi}\left[-0.5 - \frac{(1-\xi^2)}{4\xi} ln\left|\frac{1+\xi}{1-\xi}\right|\right] \tag{2.21}$$

Here, k_F is fermi wave vector. $\xi = \frac{\left(k^2+k_F^2+2(IE)\right)^{1/2}}{k_F}$, $k = \frac{8\pi^2 mE_i}{h^2}$. The ionisation energy of the target is denoted by (IE).

Due to the emergence of multiple inelastic events with rising of the energy, V_{ex} is dominant at lower energies and begins to diminish as energy rises. Furthermore, at a greater radial distance, the exchange potential's contribution becomes weaker.

Absorption potential

The absorption potential, V_{ab} represented by the imaginary component of the complex potential V_c in equation 2.14, is responsible for all the scattered flux losses across all the permissible pathways of electronic excitations and ionisations. The quasi-free, dynamic V_{ab} reported by Staszewska *et.al.* [10], has non-empirical expression as,

$$V_{ab}(r, E_i) = \rho(r)\left[-\sqrt{0.5T_l}\left(\frac{4\pi}{5k_F^3 E_i}\right)\theta(p^2 - k_F^2 - 2\Delta)(A_1 + A_2 + A_3)\right] \quad (2.22)$$

Here, T_l is local kinetic energy of the projectile electron given by, $T_l = E_i - V_s - V_{ex}$ and Heaviside step-function is denoted as $\theta(x)$.

$$A_1 = \frac{5k_F^3}{2\Delta}$$

$$A_2 = \frac{k_F^3(3k_F^3 - 5p^2)}{(p^2 - k_F^2)^2}$$

$$A_3 = 2\theta(2k_F^2 + 2\Delta - p^2)\frac{(2k_F^2 + 2\Delta - p^2)^{2.5}}{(p^2 - k_F^2)^2} \quad (2.23)$$

With inelastic channels, viz., electronic excitations or ionisations, the threshold energy is set by the parameter Δ. The inelastic pathways are blocked for $E_i < \Delta$. In addition, discrete contribution of inelastic channel, i.e., excitations can occur beneath the target's ionisation threshold. To avoid a disproportionate lost flux into inelastic pathways at the intermediate energy, an energy dependent form for Δ, as provided below is therefore required to achieve the desired results,

$$\Delta(E_i) = 0.8(IE) + \beta[E_i - (IE)] \quad (2.24)$$

To calculate β, $\Delta = (IE)$ at $E_i = E_P$ (energy at which the Q_{inel} is highest). After E_P, Δ is held at a constant and is made to be equal to IE (ionisation energy).

2.2.2 Partial wave analysis

The final complex potential defined as above (equation 2.14) then incorporates into the Schrödinger equation, and final Schrödinger equation is solved through the partial wave analysis method by computing the phase shifts. Partial wave analysis primarily pertains to the potentials who are spherically symmetric. The system is perfectly symmetrical in the incidence direction when the potential is spherical. As a result, the wave function and $f(\theta, \varphi)$ are purely reliant on θ and are unaffected by φ.

Pure elastic scattering

A universal solution of the Schrodinger equation can be written as

$$\Psi(r) = \sum_{lm} C_{lm} \mathcal{R}_{lk}(r) \gamma_{lm}(\theta, \varphi) \tag{2.25}$$

In this case, $m = 0$ since the system does not change with respect to the φ, an azimuthal angle. Additionally, under these circumstances, $\gamma_{lm}(\theta, 0) \sim P_l(\cos\theta)$. As a result, the above equation of $\Psi(r)$ will be,

$$\Psi(r, \theta) = \sum_{l=0}^{\infty} a_l \, \mathcal{R}_{lk}(r) \; P_l(cos\,\theta) \tag{2.26}$$

Each of these terms, referred to as a *partial wave*, is an eigenfunction of L_Z and L^2operators.

Considering the incident part of the equation 2.6 as a superposition of the eigenstates of angular momentum operators,

$$\Psi(r, \theta) \cong \sum_{l=0}^{\infty} i^l (2l + 1) j_l(kr) P_l(cos\,\theta) + f(\theta) \frac{exp\,(ikr)}{r} \tag{2.27}$$

Now, at the asymptotic region, this $\Psi(r, \theta)$ has the form as follow by considering the Bessel function, $j_l(kr)$ at $r \to \infty$,

$$\Psi(r, \theta) \simeq \sum_{l=0}^{\infty} i^l (2l + 1)\, P_l(cos\,\theta) \frac{sin\left(kr - \frac{\pi}{2} l\right)}{kr} + f(\theta, \varphi) \frac{exp\,(ikr)}{r} \tag{2.28}$$

$$\Psi(r, \theta) \simeq -\frac{exp\,(-ikr)}{2ikr} \sum_{l=0}^{\infty} i^l (2l + 1)\, P_l(cos\,\theta) + \frac{exp\,(ikr)}{r} \left[f(\theta) + \frac{1}{2i} \sum_{l=0}^{\infty} (-i)^l (i)^l (2l + 1) P_l(cos\,\theta) \right] \tag{2.29}$$

$$\text{where, } \sin\left(kr - \frac{\pi}{2} l\right) = \frac{e^{ikr}(-i)^l - e^{-ikr}(i)^l}{2i} \tag{2.30}$$

Now, the radial term of $\Psi(r, \theta)$ from equation 2.26, should satisfy the radial equation and as the asymptotic region is of relevance, the equation will be,

$$\left[\frac{d^2}{dr^2} + k^2 - \frac{8\pi^2 m}{h^2} V(r) - \frac{l(l+1)}{r^2}\right] (r\mathcal{R}_{lk}(r)) = 0 \tag{2.31}$$

$$\left[\frac{d^2}{dr^2} + k^2\right] (r\mathcal{R}_{lk}(r)) = 0 \tag{2.32}$$

Here, for deriving the above equation, the fact that $V(r)$, potential will be 0 at the large distance, has been taken into consideration.

By using the Neumann functions, $\eta_l(r)$ and Bessel functions, $j_l(r)$, the generalized solution of equation 2.32 can be written as,

$$\mathcal{R}_{lk}(r) = D_l \, j_l(r) + E_l \, \eta_l(r) \tag{2.33}$$

And asymptotic form of the $\mathcal{R}_{lk}(r)$ can be derived by considering the asymptotic values of $\eta_l(r)$ and $j_l(r)$, as

$$\lim_{r\to\infty} \mathcal{R}_{lk}(r) \to D_l \frac{sin\left(kr-\frac{\pi}{2}l\right)}{kr} - E_l \frac{cos\left(kr-\frac{\pi}{2}l\right)}{kr} \tag{2.34}$$

Take, $C_l = \sqrt{D_l^2 + E_l^2}$ and $\tan(\delta_l) = -\frac{E_l}{D_l}$

Then, $\mathcal{R}_{lk}(r)$ at asymptotic region,

$$\lim_{r\to\infty} \mathcal{R}_{lk}(r) \to C_l \frac{sin\left(kr-\frac{\pi}{2}l+\delta_l\right)}{kr} \tag{2.35}$$

Here, δ_l, a fingerprint of the scattering system, is known as *phase shift*. It is expected that cross sections will be dependent on this δ_l. Solving the Schrödinger equation in the area $r < a$, where a is the bounded range of the potential $V(r)$, will allow for the numerical determination of these phase shifts. As a result of the boundary condition, it is anticipated that the $\mathcal{R}_{lk}(r)$, as well as its derivative and logarithmic derivative, will be continuous when $r = a$. Thus, for $r = a$, we have

$$\mathcal{R}_l(k,r) = D_l(k)\, tan\, \delta_l(k) \left[\frac{j_l(k,r)}{tan\, \delta_l(k)} - \eta_l(k,r)\right]_{r=a} \tag{2.36}$$

Then, at $r = a$, $\mathcal{R}_l^{-1} \frac{d\mathcal{R}_l}{dr} = k \left[\frac{\frac{dj_l(k,r)}{dr} - \frac{d\eta_l(k,r)}{dr}\tan\delta_l(k)}{j_l(k,r) - \eta_l(k,r)\tan\delta_l(k)}\right]$

Hence, phase shift, δ_l can be obtained from,

$$tan\, \delta_l(k) = \left[\frac{k\frac{dj_l(ka)}{dr} - j_l(ka)\,\mathcal{R}_l^{-1}\frac{d\mathcal{R}_l}{dr}}{k\frac{d\eta_l(ka)}{dr} - \eta_l(ka)\,\mathcal{R}_l^{-1}\frac{d\mathcal{R}_l}{dr}}\right] \tag{2.37}$$

Now, from the equation 2.35, the $\Psi(r,\theta)$ from equation 2.26 can be written as,

$$\lim_{r\to\infty} \Psi(r,\theta) \simeq \sum_{l=0}^{\infty} a_l(r) P_l(cos\,\theta) \frac{sin\left(kr-\frac{\pi}{2}l+\delta_l\right)}{kr} \tag{2.38}$$

This is the deformed plane wave, which can be distinguished from the incidence wave by a phase shift, δ_l. An alternative formulation of the above equation is as,

$$\Psi(r,\theta) \to -\frac{exp(-ik\ )}{2ikr}\sum_{l=0}^{\infty} a_l i^l\, exp(-i\delta_l)\, P_l(cos\,\theta) + \frac{exp(ikr)}{2ikr}\sum_{l=0}^{\infty} a_l(-i)^l\, exp\,(i\delta_l)\, P_l(cos\,\theta) \tag{2.39}$$

Now, from equation 2.29 and 2.39, by equating the coefficient of term, $\frac{\exp(-ikr)}{r}$

$$f(\theta) = \frac{1}{2ik}\sum_l (2l+1)P_l(cos\,\theta)\,(exp(2i\delta_l) - 1) \quad (2.40)$$

where, $e^{2i\delta_l(k)}$ is defined as the S-matrix (scattering matrix) and $|S_l(k)| = \left|e^{2i\delta_l(k)}\right| = 1$ for pure elastic case.

Now, Q_T can be derived from $f(\theta)$ as,

$$Q_T = \sum_l Q_l = \frac{4\pi}{k^2}\sum_l^{\infty}(2l+1)\,sin^2\delta_l \quad (2.41)$$

where, Q_l represents the cross section for each partial wave corresponding to different angular momentum states.

Let's now determine whether our proposed solution satisfies optical theorem. From equation 2.40,

$$f(0) = \frac{1}{k}\sum_{l=0}^{\infty}(2l+1)\,(sin\,\delta_l\,cos\,\delta_l + isin^2\delta_l) \quad (2.42)$$

Hence, $Q_T = \frac{4\pi}{k}Im[f(0)] = \frac{4\pi}{k}\sum_l^{\infty}(2l+1)\,sin^2\delta_l$ (2.43)

Therefore, we conclude that the condition holds, and since scattering reduces the particles in the incident beam, the total cross section, Q_T is proportional to this reduction.

Inelastic scattering

When dealing with inelastic scattering, it is important to account for how the flux is absorbed by various inelastic channels. For this, the complex form of phase shifts has been introduced and hence,

$$S_l(k) = \eta_l(k)e^{2i\,Re(\delta_l)} \quad (2.44)$$

Here, $\eta_l = e^{-2\,Im(\delta_l)}$ is inelasticity factor with values $0 \leq \eta_l \leq 1$.

Hence, now the $f(\theta)$, scattering amplitude with the inelastic channel involved will be,

$$f(\theta) = \frac{1}{2ik}\sum_l (2l+1)\,[exp(2i(Re\delta_l + iIm\delta_l)) - 1]P_l(cos\,\theta) \quad (2.45)$$

Then, the elastic, inelastic and total cross sections can be given as,

$$Q_{inel}(k) = \frac{\pi}{k^2}\sum_l (2l+1)\,(1 - e^{-4\,Im(\delta_l)}) \quad (2.46)$$

$$Q_{el}(k) = \frac{\pi}{k^2}\sum_l (2l+1)\,(exp(2i(Re\delta_l + iIm\delta_l)) - 1)^2 \quad (2.47)$$

$$Q_T(k) = \frac{\pi}{k^2}\sum_l (2l+1)\,[1 - \eta_l\,cos(2\delta_l)]^2 \quad (2.48)$$

Therefore, we conclude that a suitable potential $V(r)$ is required that can represent the whole scattering system, and wherefore the phase shifts can be derived to calculate the cross sections.

2.2.3 Numerov Method

The procedure for solving the Schrödinger equation, once the interaction potentials have been obtained, is described in this subsection. The famous multi-step Numerov method is employed here to solve the 2nd order differential equations. The requirement that must be met in this scenario is that the differential equation must not contain a 1st order differential term. By modifying the following terms in equation 2.31,

$$\mathcal{u}_l(k,r) = r\mathcal{R}_l(k,r) \;\; and \; G(r) = -2[E_i - V(r)] + \frac{l(l+1)}{r^2} \tag{2.49}$$

The radial equation 2.31 will be as,

$$\frac{d^2\mathcal{u}}{dr^2} - G(r)\mathcal{u} = 0 \tag{2.50}$$

The above differential equation can be seen as an analogue to a one-dimensional Schrodinger equation, making it an excellent candidate for the implementation of the Numerov technique. In addition, r fluctuates continuously from 0 to ∞; hence, in order to arrive at a numerical solution, this continuous fluctuation is transformed into extremely short finite intervals h; therefore, $r = 0, h, 2h, \ldots, \infty$. For a given value of r, we can now employ the Numerov method to determine $\mathcal{u}$.

$$\mathcal{u}_{i+1} = \frac{h^2 G_i \mathcal{u}_{i+2}\left(1-\frac{h^2}{12}G_i\right)\mathcal{u}_i - \left(1-\frac{h^2}{12}G_{i-1}\right)\mathcal{u}_{i-1}}{1-\frac{h^2}{12}G_{i+1}} \tag{2.51}$$

This formula is used to determine $\mathcal{u}_{i+1}$ recursively if the previous solutions were $\mathcal{u}_i$ and $\mathcal{u}_{i-1}$. In a similar fashion, further solutions such as $\mathcal{u}_{i+2}, \mathcal{u}_{i+3}, \mathcal{u}_{i+4}$, ... can be computed. The higher order functions of $\mathcal{u}$ can be calculated by applying the above equation once appropriate initial solutions have been selected for the functions $\mathcal{u}_0$ and $\mathcal{u}_1$. We've set h to be between $0.001a_o$ and $0.01a_o$ for this study. However, the impact energy and the system considerations dictate the mesh size h that should be used. The derivative of the $\mathcal{u}$ at $r = d$ has also been calculated with the help of the numerical differentiation formula. The value of log derivative $\left(\mathcal{R}_l^{-1}\frac{d\mathcal{R}_l}{dr}\right)$ can be determined using both $\mathcal{u}$ and its derivative. So, the usual formalism given in equation 2.37 can be utilised to determine the phase shifts, δ_l for a given

potential. It is common practise in such numerical approaches to iteratively adjust values of parameters like d and h until the convergence is reached in δ_l and cross sections. It is important to notice that as the energy of the incident electron increases, a greater number of partial waves are needed for the solution to converge. For electron scattering, for instance, 18 partial waves were employed at 20 eV for solution to converge, whereas as many as 50 were used for the same purpose between 300-5000 eV.

2.2.4 Condensed/Aqueous phase computation

The methodology that was developed and discussed in this chapter is for the gaseous phase is for gaseous phase target system and hence, is not appropriate for the calculation of the aqueous or condensed phase. When dealing with the phases other than gaseous, the target cannot be seen as an autonomous entity; rather, it is necessary to take into account the impacts of its neighbourhood. When the projectile energy is equivalent to the first ionisation energy (IE) of the molecular target, the outermost electron will be expelled from the molecule while it is in its free phase. This means that the e-molecule interaction begins to undergo inelastic processes at the threshold value, IE. This problem is especially tricky in a liquid, aqueous or a condensed substance. Ionisation does not take place until the projectile's impact energy is greater than IE, by an amount that is equivalent to the energy-band gap, denoted by E_{gap} [11,12]. To put it another way, the ionisation threshold value will be $\Delta = IE + E_{gap}$.

With this modified Δ (equation 44), the final V_{opt} is formulated with the new threshold value, which then fed into the time-independent Schrödinger equation. This Schrödinger equation is then solved utilising the partial wave analysis method through computing the complex scattering phase shifts, δ_l. A phase shift is consequently created for each partial wave that contains information about the collision process. The resulting phase shift is used to determine the Q_{inel} using the scattering matrix ($S_l(k) = e^{2i\delta_l(k)}$) as seen before in case of the gaseous phase target systems.

For the present work, we have computed the inelastic and ionisation cross sections for the aqueous DNA constituents. In addition to cross-sections, we have also determined the inelastic mean free path, abbreviated as IMFP, for the various inelastic processes that have been explored here. The equation illustrates the relationship between the IMFP and the inelastic cross sections, can be given as,

$$\lambda_{inel} = \frac{1}{NQ_{inel}} \tag{2.52}$$

In which, N is the number density of the aqueous or condensed target system, expressed as $N = \frac{N_A \rho}{M}$. Here, M is the molecular mass, ρ is the target material density and N_A is the avogadro's number.

Further, the electron stopping power or energy loss per unit path length of electron in the target medium $\left(\frac{dE}{dx}\right)$ is also evaluated in terms of mass stopping power $\frac{1}{\rho}\left(\frac{dE}{dx}\right)$, which takes into account the density of the medium from the following equation [13],

$$-\frac{1}{\rho}\left(\frac{dE}{dx}\right) = \frac{N_a}{M}\bar{E}Q_{inel} \tag{2.53}$$

where, $\bar{E}$ is mean excitation energy of the aqueous or condensed target system.

When the particle penetrates the distance r that the particle travelled in the medium, the absorbed dose, D is also obtained from the following equation at the distance [14,15],

$$D = \frac{-\left(\frac{dE}{dx}\right)}{4\pi\rho\ ^2} \tag{2.54}$$

All of these applied quantities are significantly essential in the modelling of the DNA damage assessment and since human body believed to be consists of about 70% water, the DNA materials are always found to be covered with those water molecules through hydrogen bonding [16,17]. Therefore, for the present calculation, we considered the aqueous DNA compounds to deal with the more realistic picture of it. The computed results for this case can be found in the chapter V of this thesis.

2.2.5 Two-parameter semi-empirical method (2p-SEM)

Earlier work examined the Q_T's dependency on impact energy for both moderate [18,19] and high energies [20,21] and provided the following formula,

$$Q_T = \frac{A}{E^B} \tag{2.55}$$

where the value of parameter A is determined by the molecular properties, such as the size of the molecule and its polarisability. The value of B at high energies, above 500 eV, will be ~0.7, as suggested by Joshipura and Vinodkumar [21]; and García and Manero [20], but this will be the case only for smaller molecules, that is, for ten electrons (Z = 10) and up to Z = 22 electron systems, respectively. On the other hand, Nishimura and Tawara [22] suggested that

the value of *B* should be ~0.5 for the intermediate energy range of 50-500 eV. In this study, we have generated a single expression from our prior work [23] and from our current results for C_4F_7N. This expression is appropriate for the more complicated and larger molecules with Z values ranging from 55 to 95. The energy range that this expression covers is from 50 to 5000 eV.

Table 2.1 Parameters vide equation (2.55)

Parameter	Adenine ($C_5H_5N_5$) (I)	Perfluoroisobutyronitrile (C_4F_7N) (II)	Thymine ($C_5H_6N_2O_2$) (III)	Cytosine ($C_4H_5N_3O$) (IV)	Uracil ($C_4H_4N_2O_2$) (V)
A	43.47	53.64	40.75	31.70	28.33
B	0.61	0.60	0.60	0.59	0.60

Larger molecules with Z values between 56 and 94 are tabulated for both *A* and *B* in table 2.1, and it can be seen that the value of *B* (~0.6) is roughly the same for all the molecules. Although A varies from molecule to molecule, this variation suggests that it is dependent on the number of target electrons (Z) and polarizability (α).

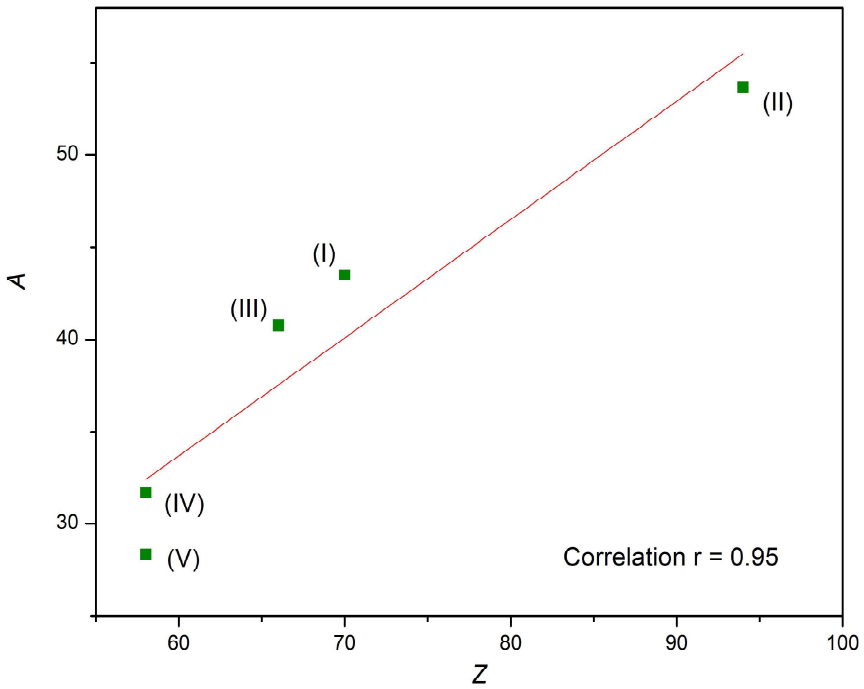

Figure 2.2 Parameter A vs Z

In order to investigate this relation, we drew the graph of A versus Z that is presented in figure 2.2. The following equation is a representation of the linear relationship that can be seen from this figure 2.3,

$$A(Z) = 0.6413Z - 4.8016 \tag{2.56}$$

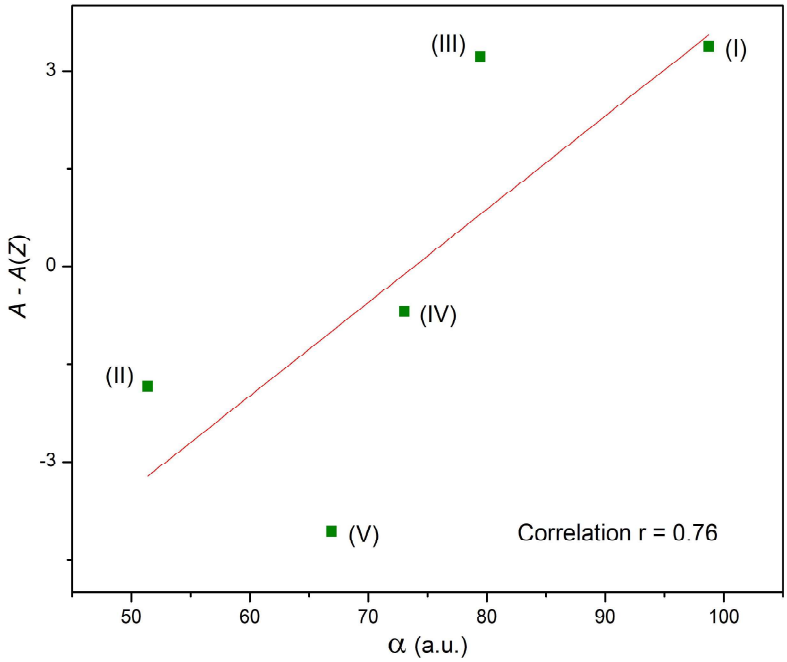

Figure 2.3 A - A(Z) vs α

However, for a given Z, the precision can be improved by incorporating the polarizability by taking into consideration the difference between the actual values of 'A' (from table 2.1) and those derived from equation 2.59 for each molecule. The dependence of this deviation ($A - A(Z)$) on the molecule size in terms of the polarisability (α) was observed. The formula for the linear relationship, which can be derived from figure 2.3, is as follows:

$$A - A(Z) = 0.1431\alpha - 10.5712 \text{ } \textit{(Correlation r = 76\%)} \tag{2.57}$$

As a result, a two-parameter expression for Q_T may be derived across the broader energy range of 50-5000 eV for large molecules using equations 2.58 to 2.60,

$$Q_T(E_i, Z, \alpha) = \frac{0.6413 \quad .1431\alpha - 15.3728}{E_i^{0.60}} \tag{2.58}$$

The energy dependence of the impact energy is noted here as $E_i^{0.60}$. The two-parameter expression found in equation 2.61, is valid for complex and heavier molecules with Z values between 55 and 95, as well as for a wider spectrum of incident energy between 50 and 5000 eV. This 2p-SEM method yields total cross sections as well as total elastic cross sections for larger and more complicated molecules. It has the potential to be highly beneficial in situations where experimental data are difficult to get, such as in the case of aqueous DNA molecules, which is an example that is readily apparent.

2.3 Complex Scattering Potential-ionisation contribution method (CSP-ic)

When it comes to electron collision processes, Q_T and the ionisation cross section (Q_{ion}) are the key cross sections of importance from an applied perspective. There is no method that can reliably calculate Q_{ion} based on Q_{inel}. To get the total ionisation cross sections out of the total inelastic cross sections, we have started using a novel semi-empirical approach called Complex Scattering Potential - ionisation contribution (CSP-ic). To obtain the total ionisation cross sections, the majority of the traditional theories, such as Deutsch-Mrk formalism (DM) and Binary-Encounter-Bethe (BEB), use shell-wise calculations and add them all up. This approach, on the other hand, is unique. Even more impressively, the overall inelastic cross section includes contributions from all plausible continuous and discrete inelastic events, viz., ionisations and excitations, respectively and hence,

$$Q_{inel}(E_i) = \sum Q_{exc}(E_i) + Q_{ion}(E_i) \tag{2.59}$$

Since the entire ionisation cross section is already included in the total inelastic cross sections, this can be used as a basis for the current approach. The other intriguing aspect is that it yields the total electronic excitation cross section (ΣQ_{exc}) as a consequence.

2.3.1 Ionisation contribution

The ionisation contribution from Q_{inel} is calculated using the standard CSP-ic technique. Joshipura and his colleagues [24] were the ones who developed this semi-empirical method. As a by-product, in addition to obtaining Q_{ion}, one additionally acquires the electronic excitation cross section, Q_{exc}. In equation 2.49, the first term disappears very quickly if $E_i \gg IE$, and in comparison, to the second term, it is rendered meaningless. The preceding

equation 2.49 makes it simple to determine that $Q_{inel} \geq Q_{ion}$, with Q_{inel} serving as Q_{ion}'s upper limit.

2.3.2 Evaluation of Q_{ion}

The above inequality $Q_{inel} \geq Q_{ion}$, serves as the basis for CSP-ic approach by defining the ratio $R(E_i) = \frac{Q_{ion}(E_i)}{Q_{inel}(E_i)}$, which must be a continuous function of energy,

$$R(E_i) = 1 - f(\cup) = 1 - c_1 \left(\frac{c_2}{\cup + a} + \frac{ln\cup}{\cup}\right) \tag{2.60}$$

with $0 \leq R(E_i) \leq 1$. In the above equation, $\cup$ is expressed as a dimensionless parameter, $\cup = {E_i}/{(IE)}$. With such a form, the energy dependency of the discrete excitations and continuous ionisation contribution at various energies is strengthened. The first item within the bracket ensures this at lower energy side, whereas the second term indicates the decrease of $\sum Q_{exc}$ at higher energy side as ${\ln\cup}/{\cup}$. Therefore, in this high energy range, the decay of function $f(\cup)$ should be proportional to ${\ln\cup}/{\cup}$. This is supported by the fact that as energy rises, the ionisation contribution rises as well, reaching unity at sufficiently high energies while the excitation channel contribution decreases to almost zero. The indicated version of the energy dependent ratio (equation 48) effectively implements the aforementioned behaviour.

The boundary conditions that must be satisfied by $R(E_i)$ are,

$$R(E_i)\begin{cases} = 0, \ f(\cup) = 1, & for\ E_i \leq IE \\ = 1, \ f(\cup) \approx 0, & for\ E_i \gg IE \\ = R_P, \ 1 - f(\cup_P), & for\ E_i = E_P \end{cases} \tag{2.61}$$

These criteria are physically true due to the fact that in order for the target to ionise, energy greater than IE is required. Ionisation cannot take place below this energy, which demonstrates that the first criterion has been met. Similar to the first requirement, the second one is easily satisfied because, at higher energy, the participation of the ionisation channel in the inelastic process predominates over the excitation processes. As a result, the ratio moves towards unity in this condition. However, the last condition is inferred from experiments showing that the ionisation contribution is 70%-80% at the inelastic cross section peak [25,26]. While this does increase the uncertainty in calculating the direct Q_{ion} by about ±7%,

it is still significantly smaller than the experimental uncertainty, which typically ranges from about 10% to 15%. The selection of a constant ratio on the other hand, ensures the reproducibility and consistency of the current procedure. The calculation of this ratio cannot be determined with absolute certainty because there is no standard procedure, and the value of R_P may also change depending on the target system. However, the generalizability of the procedure is not compromised in any way by the choice of 0.7 to 0.8 presented here.

2.3.3 Summed total electronic excitation cross-sections (ΣQ_{exc})

As seen previously, the main contributors of the total inelastic processes are ionisation and electronic excitation processes for the energy range from molecular ionisation energy to 5000 eV (equation 2.49). The electronic excitation cross-sections, Q_{exc} is computed through the equation 2.49 once the Q_{ion} is determined from the Q_{inel} by following the above methodology of CSP-ic technique. This Q_{exc} attains its peak at around 40 eV and reduces quickly above the energies 500 eV.

2.4 Correlation study: Prediction of polarisability (α) and dielectric constant (ε)

For the purpose of computing useful target properties such as polarisability (α) and dielectric constant (ε), we have made use of the Q_{ion} that have been computed for the target systems.

2.4.1 Polarisability (α)

According to the qualitative dependency nature of the maximum ionisation cross-sections, Q_{ion}(peak) that Harland provided, with the target's polarisability (α) [27],

$$Q_{ion}(peak) = \frac{e}{4\varepsilon_o}\sqrt{\frac{\alpha}{\Delta}} \tag{2.62}$$

When the target system is in its gas phase, according to Harland, Δ will be equal to *IE*. While we defined, $\Delta = IE + E_{gap}$ for condensed or solid phase species since this is where the ionisation of the system happens only when the incoming energy exceeds the $\Delta = IE + E_{gap}$ threshold value.

2.4.2 Dielectric constant (ε)

The two formulae for the dielectric constant (ε) have been developed by leveraging the dependency of the Q_{ion}(peak) on α and ε values. The first formulation of dielectric constant as a function of Q_{ion}(peak) that was proposed and determined by using the dependence of Q_{ion}(peak) with α (equation 2.62) and the Clausius-Mosotti (CM) equation [27],

$$\frac{\varepsilon-1}{\varepsilon+2} = C \cdot (Q_{ion}(peak))^2 N\Delta \tag{2.63}$$

where, N is the number density of the molecule and C is the constant = $\frac{64\pi}{3}\left(\frac{\varepsilon_o}{e}\right)^2$.

Secondly, the Onsager dielectric equation [28,29], which works well for the case of liquids is given by,

$$\frac{\varepsilon-1}{\varepsilon+2} = \frac{4\pi}{3}\alpha N + \frac{(\varepsilon-\varepsilon_\infty)(2\varepsilon+\varepsilon_\infty)}{\varepsilon(\varepsilon_\infty+2)^2} \tag{2.64}$$

This equation is thought to be more applicable in the aqueous phase study, and again the equation of dielectric constant as a function of Q_{ion}(peak) is proposed as,

$$\frac{\varepsilon-1}{\varepsilon+2} = C \cdot (Q_{ion}(peak))^2 N\Delta + \frac{(\varepsilon-\varepsilon_\infty)(2\varepsilon+\varepsilon_\infty)}{\varepsilon(\varepsilon_\infty+2)^2} \tag{2.65}$$

where, ε_∞ is the high frequency dielectric constant, which can be obtained from the CM equation,

$$\frac{\varepsilon_\infty-1}{\varepsilon_\infty+2} = \frac{4\pi}{3}N\alpha \tag{2.66}$$

2.5 Low-energy computation: R-matrix approach

In most cases, the energy of the collision may be broken down into three distinct buckets: low, moderate, and high. Areas with energies lower than the target's ionisation threshold (IE) are referred to be low energy regime. This energy regime is followed by the intermediate energy area, which covers energies up to a few multiples of IE, and then by the high energy region, which takes into account all energies above this intermediate energy zone. The physics in this area are among the most complex, and as a result, this part of the spectrum calls for extra care to handle it. Within the scope of this thesis, the low-energy electron impact scattering from difluoromethane (CH_2F_2) is investigated. To address the issue of the low energy scattering (0-15 eV), we make use of the R-matrix approach, due to the intricacy

of the procedure. The famous R-matrix formalism, which has its roots in nuclear physics, is a way to study low energy scattering. This technique calls for the space to be partitioned into two distinct regions—an inner and an outer one, which are then separated by a sphere with a radius of 'a', the centre of which is located at the centre of mass of the molecular or atomic target. Since the inner region completely accommodates the target wave function, this technique is nearly useless for studying molecules with complex geometries. In this case, the scattering electron is located in the outer region, where it is subjected to the local long-range potential resulting from the interaction with the target system. This is due to the fact that the scattering electron is located in a location that is sufficiently enough away from the target charge cloud. As a result, the correlation and exchange effects do not have any significant influence. Because of the presence of n electrons of the target system and a single scattering electron, the physics in the inner area is inherently complex. The diameter of the sphere, which ranges from $10a_o$ to $15a_o$, is decided upon in such a way that the entire target system's wave function is encapsulated within this inner spherical region. All electrons are believed to be the same in this region, making it energy independent. Because of this, the computation only needs to be done once for the inner spherical space, and this result provides the bridge between both the regions. Solving the considerably easier problems that arise in the outer region case, makes it possible to tackle the energy dependence. The R-matrix concept is elaborated upon below.

2.5.1 Methodology

Within the bounds of the fixed nuclei approximation (FNA), the general Schrodinger equation for a system with $n + 1$ particles, is given as,

$$(\boldsymbol{H} - E)\boldsymbol{w}(E) = 0 \tag{2.67}$$

In the case of a finite sphere with radius 'a', an additional term known as the Bloch term is introduced, which can be written as,

$$L(b) = \sum_{i=1}^{n+1} \frac{h^2}{2ma} \delta(r_i - a) \left[\frac{d}{dr_i} + \frac{(1-b)}{r_i}\right] \tag{2.68}$$

The boundary term and arbitrary constant, 'b' in the R-matrix often sets to be zero while maintaining the generality of the expression. Therefore, the Schrodinger equation for the cubage that can be contained within the inner spherical space ($r \leq a$) can be written as,

$$(\boldsymbol{H} + \boldsymbol{L} - E)\boldsymbol{w}(E) = \boldsymbol{L}\boldsymbol{w} \tag{2.69}$$

For the bounded interior spherical region, the Hamiltonian is $\boldsymbol{H} + \boldsymbol{L}$. The inclusion of the Bloch term maintains the Hamiltonian's hermitian character of this expression. At particular discrete energies ε_k with wave function $\boldsymbol{w_k}$, above equation holds true. Then,

$$\langle \boldsymbol{w}_k | \boldsymbol{H} + \boldsymbol{L} | \boldsymbol{w_{k'}} \rangle = \delta_{kk}\, \varepsilon_k \tag{2.70}$$

Also, the following can be written,

$$\boldsymbol{w_k}(\varepsilon) = \sum_k A_k(\varepsilon) \boldsymbol{w_k} \tag{2.71}$$

in which, the inner space wavefunction coefficient denoted by A_k is energy dependent. Now, from above two equations 2.70 and 2.71,

$$\boldsymbol{w}(\varepsilon) = \sum_k \frac{|w_k\rangle\langle \boldsymbol{w_k}|\boldsymbol{L}|\boldsymbol{w}\rangle}{\varepsilon_k - \varepsilon} \tag{2.72}$$

The preceding equation can be rewritten by substituting the Bloch operator [30] and projecting $\boldsymbol{w_k}$ on each target states (φ_i^n), as follows,

$$F_i(a) = \frac{1}{2}\sum_k \frac{w_{ik}(a)}{\varepsilon_k - \varepsilon} \sum_j w_{ik}(a) \left[r \frac{dF_j}{dr} - bF_j \right] \Big|_{r=a} \tag{2.73}$$

$$F_i(a) = \sum_j R_{ij}(a, \varepsilon) \left[r \frac{dF_j}{dr} - bF_j \right] \Big|_{r=a} \tag{2.74}$$

which implies to, $R_{ij}(a, \varepsilon) = \frac{1}{2}\sum_k \frac{w_{ik}(a) w_{jk}(a)}{\varepsilon_k - \varepsilon}$ (2.75)

The radial wave function for the outer region is denoted by the symbol $F_i(r)$, and it corresponds to the boundary amplitudes $w_{ik}(a)$ and the asymptotic channel i. The boundary form of a conventional R-matrix is given by equation 2.75. Inner-region scattering eigen energies, ε_k are singularities in this R-matrix. Equation 2.75 gives the inner boundary rule for differential equations in the outer area. This condition can be regarded as the beginning of the process of solving the problem of scattering system and the bound states. The calculation of the inner sphere supplies the necessary numerical values, namely ε_k and $w_{ik}(a)$, in order to establish the R-matrix of equation 2.75 at the boundary ($r = a$). Because these parameters do not depend on the energy, the solution to the problem of the inner spherical space only needs to be solved once for each total space spin symmetry that the collision problem possesses.

Inner spherical area

A close coupling expansion [31] can be used to demonstrate the inner part wave function for the $(n+1)$ electronic system,

$$\Psi_k^{n+1}(\boldsymbol{x}_1 \dots \boldsymbol{x}_{n+1}) = A \sum_{ij} a_{ijk}\, \varphi_i^n(\boldsymbol{x}_1 \dots \boldsymbol{x}_n)\, u_{ij}(\boldsymbol{x}_{n+1}) + \sum_i b_{ik}\, \chi_i^{n+1}(\boldsymbol{x}_1 \dots \boldsymbol{x}_{n+1}) \qquad (2.76)$$

In this calculation, the anti-symmetrization operator is denoted by the letter A, and the variational coefficients are denoted by b_{ik} and a_{ijk}. $\boldsymbol{x}_n$ is the spin and spatial coordinates of the n^{th} target molecular electron, and the wave function of the i^{th} molecular state is termed by φ_i^n. To represent the scattering e^-, the continuum orbitals is defined here as u_{ij}. These continuous orbitals, u_{ij} are located precisely where the molecule's center of mass. In addition to this, these orbitals range far enough that they are not eliminated at the boundary of the R-matrix. The short-range polarisation effects and orthogonality relaxation is involved in such arrangements. The i^{th} $n+1$ electron $\boldsymbol{L^2}$ state function is denoted by χ_i^{n+1}, where all $(n+1)$ electrons are assigned to the virtual occupied molecular orbitals. The molecular states represented by CI expansion, are carried over into the first summation of the aforementioned equation. Further, there is one electron in a continuum state, while the others move in the accessible molecular orbitals, which results in the generation of "molecular target + continuum" configurations. Short range correlation and polarisation effects are taken care via a summation in the second term that runs across the configurations χ_i^{n+1}, which relies on the geometry of the molecule in question and have zero amplitude on the R-matrix border. Additionally, the orthogonality between the molecular target orbitals and continuum orbitals, u_{ij} is relaxed as a result of these χ_i^{n+1} functions.

The continuum basis functions are represented as a partial wave expansion using polar coordinates (r, θ, ϕ) so that they can correctly match the asymptotic channels in the outer region,

$$\mathfrak{x}_{ij}(r, \theta, \phi) = f_{ij}(r) Y_{l_i, m_i}(\theta, \phi)\, \Xi_{1/2} \qquad (2.77)$$

Here, $\Xi_{1/2}$ is the electron spin function.

At the boundary

In order to construct the R-matrix at the boundary line ($r = a$), the pole locations and amplitude at the boundary must be known. The overlap integral used to calculate this amplitude at $r = a$ for any i^{th} channel,

$$w_{ik}(a) = \left\langle \varphi_i^n Y_{l_i,m_i} \Xi_{1/2} \middle| \Psi_k^{n+1} \right\rangle \tag{2.78}$$

Alternately, one could compute $w_{ik}(a)$ using the u_{ij} and the inner region wave function coefficients, a_{ijk} from

$$w_{ik}(a) = \sum_j u_{ij}(a) a_{ijk} \tag{2.79}$$

Hence,

$$F_i(a) = \sum_k A_k(\varepsilon) w_{ik}(a) \tag{2.80}$$

The energy-dependent impact particle wave function is then provided for the i^{th} channel at the boundary line ($r = a$). After it has been calculated, other information that is significant for the computation of the outer space, which is essentially the molecule properties, are derived here [32].

Outer configuration space

The wave function associated with this outer part of the configuration space will be,

$$\Psi^{n+1}(\varepsilon) = \sum_{i=1}^{n} \varphi_i^n(\boldsymbol{x}_i, \dots, \boldsymbol{x}_n)\, F_i(r_{n+1}) Y_{l_i,m_i}(\theta, \phi)\, \Xi_{1/2} \tag{2.81}$$

In this case, the summation is performed across all the n-channels that are linked to every target molecular states. After plugging the equation 2.81 into the Schrödinger equation,

$$-\left[\frac{d^2}{dr^2} - \frac{l_i(l_i+1)}{r^2} + k_i^2\right] F_i(r) = 2 \sum_{j=1}^{n} V_{ij}(r)\, F_j(r) \tag{2.82}$$

Thus, $F_j(r)$, radial function is represented by the system of n homogeneous, coupled differential equations [33]. In the above equation, $k_i = \sqrt{2(\varepsilon - \varepsilon_i^n)}$, is the wavenumber of the scattering electron consorted with the i^{th} channel. The difference in the energy between the ground state of the molecular target and the scattered electron, is $(\varepsilon - \varepsilon_i^n)$. The channel is open if and only if k_i is positive; otherwise, it is closed. Furthermore, V_{ij} is the long-range effective potentials in this region, which are determined from the target molecular attributes.

$$V_{ij}(r) = \sum_{\lambda=0} \frac{\alpha_{ij}^{(\lambda)}}{r^{\lambda+1}} \tag{2.83}$$

In which, $\alpha_{ij}^{(\lambda)} = \sqrt{\frac{2l_i+1}{2l_j+1}}\, C\left(l_i \lambda l_j; m_i m_\lambda m_j\right) C(l_i \lambda l_j; 000) Q_{ij}^{(\lambda)}$ (2.84)

are the coefficients for asymptotic potential of the order (λ). The Clebsch-Gordan coefficients are denoted here as $C\left(l_i \lambda l_j; m_i m_\lambda m_j\right) C(l_i \lambda l_j; 000)$ and $Q_{ij}^{(\lambda)}$ are the molecular state moment. Here, for charged target systems, $\lambda = 0$; for quadrupole $\lambda = 2$ and for dipole $\lambda = 1$. When there is a permanent moment, then $i = j$.

After that, we extend the R-matrix from $r = a$ to $r = r_f$ [34,35], where r_f is a sufficiently larger distance that we may ignore the non-coulombic interaction in the asymptotic area ($r > r_f$). Although there are a number of approaches [36–39] that can be used to obtain these asymptotic solutions, the Gailitis procedure [39] is the one that is utilised in this study because it is thought to be the most reliable approach out of all the existing ones. Therefore, the solution to equation 2.82 in the ($r > r_f$) region is expressed as,

$$F_{ij} \sim \frac{1}{\sqrt{k_i}} \left(sin\, \theta_i\, \delta_{ij} + cos\, \theta_i\, K_{ij}\right) \tag{2.85}$$

K_{ij} constructs a **K**-matrix that is real and symmetric; and contains all of the scattering information. θ_i is defined as channel angle,

$$\theta_i = \begin{cases} k_i r - \frac{\pi l_i}{2}, & for\ neutral\ target \\ k_i r - \frac{\pi l_i}{2} - \eta_i\, ln(2rk_i) + \sigma_i, & if\ Z - N \neq 0 \end{cases} \tag{2.86}$$

where, $\eta_i = \frac{Z-N}{k_i}$ and the coulomb phase, $\sigma_i = arg(\Gamma(1 + l_i + i\eta_i))$ (2.87)

The calculations of the eigen phase sum is done by,

$$\delta(\varepsilon) = \sum_i tan^{-1}(K_{ii}^D) \tag{2.88}$$

where K_{ii}^D is the set of eigenvalues that the **K**-matrix has. The scattering matrix, also known as **S**-matrix, and transition matrix, often known as the **T**-matrix, can both be constructed with the assistance of the **K**-matrix.

$$\boldsymbol{S} = \frac{1+i\boldsymbol{K}}{1-i\boldsymbol{K}} \text{ and } \boldsymbol{T} = \boldsymbol{S} - 1 \tag{2.89}$$

And finally, the cross section can be calculated through **T**-matrix,

$$\sigma(i \to i') = \frac{\pi}{k_i^2} \sum_S \frac{(2S+1)}{2(2S_i+1)} \sum_{\Gamma ll'} \left| T_{ili'l'}^{\Gamma S} \right|^2 \quad (2.90)$$

The scattering electron has an energy of $\frac{\pi}{k_i^2}$ relative to its original state of spin angular momentum S_i. Here, l and l' represent the degenerate channels corresponds to the target's initial and final states, respectively. Γ covers all the spatial symmetries.

2.5.2 Polar molecular targets

The previous discussion on calculation of the R-matrix, only takes into account up to g-waves ($l \leq 4$). However, for polar molecules, such low l-expansions are simply not enough. For the purpose of including the higher partial derivatives in this thesis, the Born top-up approach [40] is utilised. This provides an accurate representation of the long-range interaction for molecules that have a dipolar character, and it converges the cross sections in the correct way. Since the higher partial waves (above L_m, the minimum angular momentum), are weakly scattered, the Born correction, given by following expression is useful for treating them independently.

$$\Delta Q = Q^{FBA} - Q_{Lm}^{FBA} \quad (2.91)$$

The cross section in this case, denoted by Q^{FBA} is the plane wave Born approximation cross section, and Q_{Lm}^{FBA} is the cross section calculated from a finite expansion of the first-Born cross section, which contains the same number of partial waves as Q^R (equation 2.90). The closed version of the FBA can be achieved without having to resort to a partial wave expansion, and it include contributions from all angular momenta [41]. To obtain the complete integral cross section for polar molecules, we add ΔQ (computed via equation 2.91) to Q^R (calculated through equation 2.90).

2.5.3 Scattering models used in the calculations

Since the Schrödinger equation is notoriously tricky to solve exactly, several approximations have been developed to resort in obtaining the reliable results. QUANTEMOL-N provides users with access to three distinct models, each with its own set of L^2 functions and molecular electronic states to be employed in the aforementioned equation 2.76. Let's look at the models in detail.

A. Static model

- The electrons involved in scattering and the ones in the target are treated as two distinct entities.
- Therefore, there is no possibility for the exchange.
- The perturbation brought on by polarisation effects is also not taken into account.

B. Static exchange model (SE)

- Although exchange interaction is present in this model, exclusion of polarisation effect prevents the target system from being disturbed.
- Electrons of the target system are remained immobilised in their ground state configuration, since the electronic excitations are ignored in this model.
- Since the core and Feshback excited resonances needed the excitation of the bound electrons, they remain undetectable in this model. However, shape resonance can be detected.
- Not afflicted by pseudo-resonances, therefore, suitable for onsetting the calculation.
- Compatible with high-energy calculations.

C. Static exchange with polarisation model (SEP)

- There will be a perturbation of the target system due to the consideration of correlation and polarisation effects.
- This paradigm permits the single excitations from the ground state to be incorporated into other higher orbitals.
- This method allows for the thorough study of the shape resonances, while core excited resonances are inadequately studied. Also, pseudo resonances are produced at high energies.
- Appropriate for the low energy computations.

D. Complete active space-configuration interaction model (CAS-CI)

- Compared to previous scattering models, this one is quite advanced.
- The calculation relies on the close coupling approximations.
- In order to build the target system wavefunction, all the allowed configurations are taken into consideration.
- Can detect all core excited, Feshback and shape resonances.

- The computation not only produces elastic cross sections, but also electronic excitation cross-sections.

2.5.4 Various modules of QUANTEMOL-N code

The procedure for running a target and carrying out the computations in the inner and outside region is depicted in Figure 2.4, 2.5, and 2.6. Each important module for both regions are described as follow.

Modules for inner region computation

- **SWMOL3**: calculates the one electron and two electron integrals between the numerous atomic orbitals that are produced at the beginning of the process
- **GAUSTAIL**: examines each integral's outer contribution of the R-matrix sphere and combines Bloch operator matrix components with Hamiltonian matrix elements
- **SWORD**: arranges SWMOL3 atomic integrals
- **SWFJK**: produces the different possible amalgamation of the exchange and coulomb integrals for the Fock matrix
- **SWSCF**: implementing the Hartree-Fock self-consistent field optimisation (HF-SCF), the integrals that were formed by SWFJK are used here to generate the molecular orbitals from the linear combination of the atomic orbitals
- **SWTRMO**: executes the four-index transformation from the atomic orbital representation to the molecular orbital representation of the arranged integrals acquired by SWMOL3
- **SWEDMOS**: using the orthogonalisation technique, Schmidt and symmetric orthogonalisation orbitals are combined. Along the boundary of the R-matrix, the amplitude of each continuum orbital is calculated as a function of partial wave.
- **CONGEN**: constructs the configuration state functions, often known as CSFs, using appropriate symmetry and spin couplings
- **SCATCI**: the CONGEN-generated configurations are used to build the Hamiltonian, which is subsequently diagonalised. Eigen vectors and eigen energies are computed here. The module returns ε_k^{n+1}, pole energies of the R-matrix and the corresponding wave functions φ_k^{n+1}, expressed via coefficients b_{ik} and a_{ijk}
- **GAUSPROP**: performs the necessary computations for the property integrals, as requested by DENPROP

- **DENPROP**: estimates the wave function properties and generates the transition density matrix by employing the target eigenvectors acquired from the CI-calculation. This module performs additional analysis on the diagonalized tensor component values of α_{xx}, α_{yy}, α_{zz}; dipole polarizability and multipole transition moments.

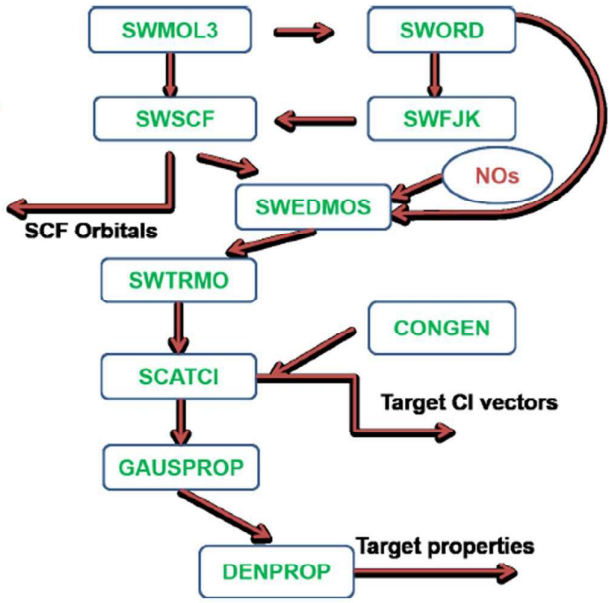

Figure 2.4 Flow diagram for inner region target calculation

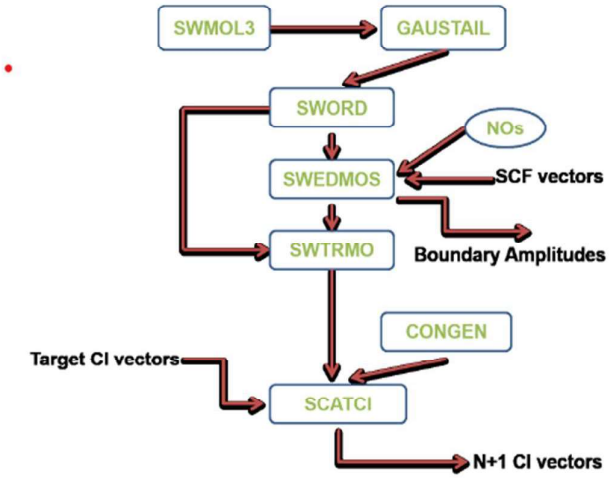

Figure 2.5 Inner area program flow diagram

Modules for outer region computation

- **SWINTERF**: It serves as the connecting mechanism between the inner and exterior region. This module takes the SWEDMOS boundary amplitudes, the eigenvectors and eigenvalues of the $n + 1$ system, and the DENPROP multipole moments as its inputs. The output of this module supplies the molecular target attributes as well as all other data that is necessary for constructing the R-matrix for exterior region.
- **BOUND**: provides the wavefunctions of the bound state
- **RSOLVE**: This is where the majority of the time-consuming calculations for the outer region are performed. Constructing the R-matrix at the interaction radius, it is propagated to the asymptotic area using RPROP to match it with the boundary conditions. The fixed-nuclei **K**-matrices are then calculated with the aid of CFASYM.
- **EIGENP**: The previously computed **K**-matrix is diagonalized in order to produce the eigen phases by computing the arctan values of their respective eigenvalues.

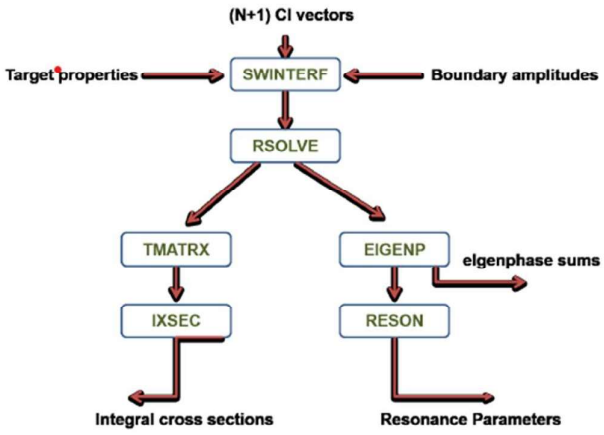

Figure 2.6 Outer area calculation flow diagram

- **PolyDCS**: cross sections for rotational excitations, momentum transfers, and differential cross sections are all provided here using the **K**-matrix.
- **TMATRX**: generates the T-matrix by applying conventional equations to the K-matrix that was provided
- **IXSEC**: From the T-matrices, the integral cross sections are computed here.

- **BORNCROS**: determines the born cross sections as well as the born correction that needs to be incorporated to the cross sections
- **RESON**: using Breit-Wigner profiles to fit eigen phase sums, resonances are found
- **TIMEDEL**: offers a different approach to the process of fitting resonances

2.6 Bibliography

[1] Charles J. Joachain, *Quantum Collision Theory* (North-Holland Pub. Co., 1975).

[2] R. Bethe, Hans A. and Jackie, *Intermediate Quantum Mechanics*, Third edit (CRC Press, Taylor and Francis group, Boca Raton, FL, 2018).

[3] Mohit Swadia, Yogesh Thakar, Minaxi Vinodkumar, and Chetan Limbachiya, *Theoretical Electron Impact Total Cross Sections for Tetrahydrofuran (C4H8O)*, The European Physical Journal D **71**, 85 (2017).

[4] M. Vinodkumar, C. Limbachiya, H. Desai, and P. C. Vinodkumar, *Electron-Impact Total Cross Sections for Phosphorous Triflouride*, Phys Rev A **89**, 062715 (2014).

[5] H. L. Cox and R. A. Bonham, *Elastic Electron Scattering Amplitudes for Neutral Atoms Calculated Using the Partial Wave Method at 10, 40, 70, and 100 KV for Z = 1 to Z = 54*, J Chem Phys **47**, 2599 (1967).

[6] N. T. Padial and D. W. Norcross, *Parameter-Free Model of the Correlation-Polarization Potential for Electron-Molecule Collisions*, Phys Rev A **29**, 1742 (1984).

[7] J. P. Perdew and A. Zunger, *Self-Interaction Correction to Density-Functional Approximations for Many-Electron Systems*, Phys Rev B **23**, 5048 (1981).

[8] X. Zhang, J. Sun, and Y. Liu, *A New Approach to the Correlation Polarization Potential-Low-Energy Electron Elastic Scattering by He Atoms*, Journal of Physics B: Atomic, Molecular and Optical Physics **25**, 1893 (1992).

[9] S. Hara, *The Scattering of Slow Electrons by Hydrogen Molecules*, J Physical Soc Japan **22**, 710 (1967).

[10] G. Staszewska, D. W. Schwenke, and D. G. Truhlar, *Investigation of the Shape of the Imaginary Part of the Optical-Model Potential for Electron Scattering by Rare Gases*, Phys Rev A **29**, 3078 (1984).

[11] S. H. Pandya, B. G. Vaishnav, and K. N. Joshipura, *Electron Inelastic Mean Free Paths in Solids: A Theoretical Approach*, Chinese Physics B **21**, (2012).

[12] K. N. Joshipura, S. Gangopadhyay, C. G. Limbachiya, and M. Vinodkumar, *Electron Impact Ionization of Water Molecules in Ice and Liquid Phases*, J Phys Conf Ser **80**, 012008 (2007).

[13] A. Muñoz, J. C. Oller, F. Blanco, J. D. Gorfinkiel, and G. García, *Electron Scattering Cross Sections and Stopping Powers in H2*, Chem Phys Lett **433**, 253 (2007).

[14] William V. Prestwich, Josane Nunes, and Cheuk S. Kwok, *Beta Dose Point Kernels for Radionucides of Potential Use in Radioimmunotherapy*, The Journal of Nuclear Medicine **30**, 1036 (1989).

[15] Sh. Mohammed, A. Trabelsi, and K. Manai, *Stopping Power, CSDA Range, Absorbed Dose and Cross Sections Calculations of F18 Simulated in Water Using Geant4 Code*, Indian J Sci Technol **11**, 1 (2018).

[16] H. Khesbak, O. Savchuk, S. Tsushima, and K. Fahmy, *The Role of Water H-Bond Imbalances in B-DNA Substate Transitions and Peptide Recognition Revealed by Time-Resolved FTIR Spectroscopy*, J Am Chem Soc **133**, 5834 (2011).

[17] Helmholtz Association of German Research Centres, *Water Molecules Characterize the Structure of DNA Genetic Material.*, https://www.sciencedaily.com/releases/2011/04/110426091122.htm#citation_apa.

[18] H. Nishimura and H. Tawara, *Some Aspects of Total Scattering Cross Sections of Electrons for Simple Hydrocarbon Molecules*, Journal of Physics B: Atomic, Molecular and Optical Physics **24**, L363 (1991).

[19] Antonio Zecca, Grzegorz P. Karwasz, and Roberto S. Brusa, *Total-Cross-Section Measurements for Electron Scattering by NH3, SiH4, and H2S in the Intermediate-Energy Range*, **45**, (1992).

[20] G. García and F. Manero, *Correlation of the Total Cross Section for Electron Scattering by Molecules with 10-22 Electrons, and Some Molecular Parameters at Intermediate Energies*, Chem Phys Lett **280**, 419 (1997).

[21] K. N. Joshipura and M. Vinodkumar, *Cross Sections and Other Parameters of E- - H2O Scattering (Ei≥50eV)*, Pramana - Journal of Physics **47**, 57 (1996).

[22] H. Nishimura and H. Tawara, *Some Aspects of Total Scattering Cross Sections of Electrons for Simple Hydrocarbon Molecules*, Journal of Physics B: Atomic, Molecular and Optical Physics **24**, L363 (1991).

[23] Minaxi Vinodkumar, Chetan Limbachiya, Mayuri Barot, Avani Barot and Mohit Swadia, *Electron Impact Total Cross Sections for Components of DNA and RNA Molecules*, Int J Mass Spectrom **360**, 1 (2014).

[24] K. N. Joshipura, B. K. Antony, and M. Vinodkumar, *Electron Scattering and Ionization of Ozone, O_2 and O_4 Molecules*, Journal of Physics B: Atomic, Molecular and Optical Physics **35**, 4211 (2002).

[25] Grzegorz P. Karwasz, Antonio Zecca, and Roberto S. Brusa, *One Century of Experiments on Electron-Atom and Molecule Scattering: A Critical Review of Integral Cross-Sections*, Rivista Del Nuovo Cimento **24**, 1 (2001).

[26] R. Basner, M. Schmidt, V. Tarnovsky, K. Becker, and H. Deutsch, *Dissociative Ionization of Silane by Electron Impact*, Int J Mass Spectrom Ion Process **171**, 83 (1997).

[27] P. W. Harland and C. Vallance, *Ionization Cross-Sections and Ionization Efficiency Curves from Polarizability Volumes and Ionization Potentials*, Int J Mass Spectrom Ion Process **171**, 173 (1997).

[28] L. Onsager, *Electric Moments of Molecules in Liquids*, J Am Chem Soc **58**, 1486 (1936).

[29] M. Valiskó and D. Boda, *Dielectric Constant of the Polarizable Dipolar Hard Sphere Fluid Studied by Monte Carlo Simulation and Theories*, Condens Matter Phys **8**, 357 (2005).

[30] Claude Bloch, *Une Formulation Unifiée de La Théorie Des Réactions Nucléaires*, Nuclear Physics **4**, 503 (1957).

[31] A. M. Arthurs and Alexander Dalgarno, *The Theory of Scattering by a Rigid Rotator*, Proc R Soc Lond A Math Phys Sci **256**, 540 (1960).

[32] J. Tennyson, *Electron-Molecule Collision Calculations Using the R-Matrix Method*, Phys Rep **491**, 29 (2010).

[33] P. G. Burke, A. Hibbert, and W. D. Robb, *Electron Scattering by Complex Atoms*, Journal of Physics B: Atomic and Molecular Physics **4**, 153 (1971).

[34] L. A. Morgan, *A Generalized R-Matrix Propagation Program for Solving Coupled Second-Order Differential Equations*, Comput Phys Commun **31**, 419 (1984).

[35] K. Baluja, P. Burke, and L. Morgan, *R-Matrix Propagation Program for Solving Coupled Second-Order Differential Equations*, Comput Phys Commun **27**, 299 (1982).

[36] M. A. Cree, *Asypck2, an Extended Version of Asypck*, Comput Phys Commun **23**, 181 (1981).

[37] M. A. Cress, *ASYPCK, a Program for Calculating Asymptotic Solutions of the Coupled Equations of Electron Collision Theory*, Comput Phys Commun **19**, 103 (1980).

[38] P. G. Burke and H. M. Schey, *Elastic Scattering of Low-Energy Electrons by Atomic Hydrogen*, Physical Review **126**, 147 (1962).

[39] M. Gailitis, *New Forms of Asymptotic Expansions for Wavefunctions of Charged-Particle Scattering*, Journal of Physics B: Atomic and Molecular Physics **9**, 843 (1976).

[40] D. W. Norcross and N. T. Padial, *The Multipole-Extracted Adiabatic-Nuclei Approximation for Electron-Molecule Collisions*, Phys Rev A (Coll Park) **25**, 226 (1982).

[41] D. K. Watson and V. McKoy, *Discrete-Basis-Function Approach to Electron-Molecule Scattering*, Phys Rev A (Coll Park) **20**, 1474 (1979).